A&A 564, A64 (2014)
DOI: 10.1051/0004-6361/201323320

Astronomy & Astrophysics

HCO, c-C_3H and CF^+: three new molecules in diffuse, translucent and "spiral-arm" clouds

H. S. Liszt[1], J. Pety[2,3], M. Gerin[4,3], and R. Lucas[5]

[1] National Radio Astronomy Observatory, 520 Edgemont Road, Charlottesville VA 22903-2475, USA
e-mail: hliszt@nrao.edu
[2] Institut de Radioastronomie Millimétrique, 300 rue de la Piscine, 38406 Saint Martin d'Hères, France
[3] Observatoire de Paris (CNRS UMR 8112), 61 av. de l'Observatoire, 75014 Paris, France
[4] LERMA/LRA, École Normale Supérieure, 24 rue Lhomond, 75005 Paris, France
[5] Institut de Planétologie et d'Astrophysique de Grenoble (UMR 5274), BP 53, 38041 Grenoble Cedex 9, France

Received 22 December 2013 / Accepted 11 March 2014

ABSTRACT

Aims. We observe molecular absorption from diffuse clouds across the 3 mm receiver band.
Methods. We used the EMIR receiver and FTS spectrometer at the IRAM 30 m telescope to construct absorption spectra toward bright extra-galactic background sources at 195 kHz spectral resolution (≈0.6 km s^{-1}). We used the IRAM Plateau de Bure Interferometer to synthesize absorption spectra of $H^{13}CO^+$ and HCO toward the galactic HII region W49.
Results. HCO, c-C_3H and CF^+ were detected toward the blazars BL Lac and 3C 111 having E_{B-V} = 0.32 and 1.65 mag. HCO was observed in absorption from "spiral-arm" clouds in the galactic plane occulting W49. The complement of detectable molecular species in the 85–110 GHz absorption spectrum of diffuse/translucent gas is now fully determined at rms noise level $\delta_\tau \approx 0.002$ at E_{B-V} = 0.32 mag (A_V = 1 mag) and $\delta_\tau/E_{B-V} \approx 0.003$ mag^{-1} overall.
Conclusions. As with OH, HCO^+ and C_2H, the relative abundance of c-C_3H varies little between diffuse and dense molecular gas, with N(c-C_3H)/N(o-c-C_3H_2) ≈ 0.1. We find $N(CF^+)/N(H^{13}CO^+) \approx 5$, $N(CF^+)/N(C_2H) \approx 0.005$–0.01 and because $N(CF^+)$ increases with E_{B-V} and with the column densities of other molecules we infer that fluorine remains in the gas phase as HF well beyond A_V = 1 mag. We find $N(HCO)/N(H^{13}CO^+)$ = 16 toward BL Lac, 3C 111 and the 40 km s^{-1} spiral arm cloud toward W49, implying $X(HCO) \approx 10^{-9}$, about 10 times higher than in dark clouds. The behaviour of HCO is consistent with previous suggestions that it forms from C^+ and H_2, even when A_V is well above 1 mag. The survey can be used to place useful upper limits on some species, for instance $N(H_2CO)/N(H_2CS) > 32$ toward 3C 111, compared to 7 toward TMC-1, confirming the possibility of a gas phase formation route to H_2CO. In general, however, the hunt for new species will probably be more fruitful at cm- and sub-mm wavelengths for the near future.

Key words. ISM: molecules – ISM: abundances – ISM: clouds

1. Introduction

Microwave and sub-mm absorption-line spectroscopy have greatly extended the inventory of molecules known to exist in diffuse molecular interstellar clouds, that is, clouds with appreciable H_2 content but $A_V \lesssim 1$ mag. Just in the past few years, sub-mm observations from the PRISMAS project using the HIFI instrument on *Herschel*, from the APEX telescope in the Atacama and the GREAT instrument on SOFIA have more than doubled the number of known species following observation of the hydrides and hydride ions of oxygen, nitrogen, sulfur, fluorine and chlorine (Gerin et al. 2012; Neufeld et al. 2012). Sub-mm observations of the familiar species CH (Gerin et al. 2010) and CH^+ (Falgarone et al. 2010; Godard et al. 2012) have allowed these species, previously seen only in the optical absorption spectra of relatively nearby stars, to be tracked across the disk of the Milky Way.

Even so, the search for new molecules and the overall effort to systematize the diffuse cloud chemistry have been seriously hindered by the narrow bandwidths that were available for high sensitivity observations of heavier polyatomic species in the microwave (cm-wave and mm-wave) domain. This impediment is gradually being overcome by new technology such as the WIDAR correlator at the Karl Guthe Jansky VLA that we used to detect l-C_3H_2 and survey the abundance of several small hydrocarbons (Liszt et al. 2012). An even larger development is the advent of the very wide-band EMIR receivers at the IRAM 30 m Telescope on Pico de Veleta, which produced the recent 1–3 mm WHISPER surveys of emission from the Horsehead nebula (Guzmán et al. 2012b; Pety et al. 2012; Gratier et al. 2013).

Here we describe a 3 mm band survey of absorption from the galactic diffuse and translucent clouds seen toward the mm-bright blazars BL Lac (E_{B-V} = 0.32 mag) and 3C 111 (E_{B-V} = 1.65 mag). As a result of this work the mm-wave absorption spectrum is now known at a detection level of 1% absorption or better over the 3 mm band and this paper reports the detection of three new species HCO, c-C_3H and CF^+, toward both objects.

The plan of this work is as follows. The observations are described in Sect. 2. In Sects. 3–5 we discuss the detection and chemistry of HCO, c-C_3H and CF^+, respectively. Section 6 is the briefest of summaries.

Table 1. Sightlines and continuum targets.

Target	l	b	E_{B-V}[a]	Flux	rms[b]	v	N(HCO)	N(c-C_3H)	N(CF^+)	N($H^{13}CO^+$)	N(C_2H)
	°	°	mag	Jy	10^{-3}	km s^{-1}	10^{12} cm^{-2}	10^{11} cm^{-2}	10^{11} cm^{-2}	10^{11} cm^{-2}	10^{13} cm^{-2}
B0415+379	161.67	–8.82	1.65	3[c]	4–6	–1	3.38(0.01)	4.63(0.18)	7.9(1.6)	2.22	8.29
B2200+420	92.59	–10.44	0.32	15[c]	1.5–2	–1	0.85(0.02)	1.62(0.05)	4.0(0.7)	0.42	0.67
W49	43.17	0.01		2.5	7	40	4.86(0.32)			3.40	7.10
W49	43.17	0.01		2.5	7	51–66	14.8(0.5)				10.4

Notes. [(a)] From Schlegel et al. (1998); [(b)] see Sect. 2.2 concerning the channel-channel line/continuum rms in the spectral sweep; [(c)] approximate, derived from pointing scans assuming 6 Jy Kelvin^{-1}.

2. Observations and data reduction

2.1. The 3 mm band EMIR spectral sweep at the 30 m

Each of three sources (see Table 1) was observed for some 20 h over the course of five days observing in 2012 August. Only the data from BL Lac (B2200+420) and 3C 111 (B0415+379) will be discussed here because the flux of B0355+508 (NRAO150) was too low to detect the new species that were seen toward the other sources. We used the broadband EMIR receiver with an FTS spectrometer at 195 kHz resolution and channel separation (0.60 km s^{-1} at 100 GHz) while observing simultaneously over both 8 GHz-wide sidebands, in much the same manner as described previously for the 1–3 mm WHISPER surveys of emission from the edge-on PDR in the Horsehead nebula (Guzmán et al. 2012a). That is, we wobble-switched the secondary mirror symmetrically with an azimuth throw of 60″ about the positions of the blazar background sources and offset the receiver local oscillator to produce continuous coverage, with some overlap, over very nearly the full receiver band. In principle, observing the 3 mm frequency band requires only two tunings. However, every frequency was observed with two different frequency settings separated by 500 MHz to allow us to remove potential ghost images arising from lines in the image side band, given that the typical rejection of the EMIR sideband separating mixers in only 13 dB (a factor 20).

The temperature scale was computed and applied in the GILDAS/MIRA software on 4 GHz chunks at a time. All other reduction steps were done in the GILDAS/CLASS software[1]. In brief, we fit the continuum and divided the spectra by the continuum baseline to yield spectra as line/continuum ratios. We baselined the spectra with a low order baseline and rejected frequency ranges whose rms variation with time was much larger than the noise level, to remove potential spikes. We then coadded the spectra and improved the baseline solution by subtracting the linear interpolation of median values computed every 50 MHz over 100 MHz.

Although we are confident that there are no other species remaining to be detected in the survey data, it is not yet entirely free of artifacts, for instance unexplained features, always downward-going, that are too broad to be real absorption in the interstellar medium and are not always present in all tunings. As a check on the validity of the data acquisition path we measured the integrated absorption for previously detected lines toward BL Lac and 3C 111 and a comparison of new and old results is shown at top in Fig. 1. Above an equivalent width of 0.3 MHz (1 km s^{-1} at 100 GHz) there is a slight tendency for the new results to be smaller, perhaps as the result of underresolving the stronger lines, hence underestimating their opacity.

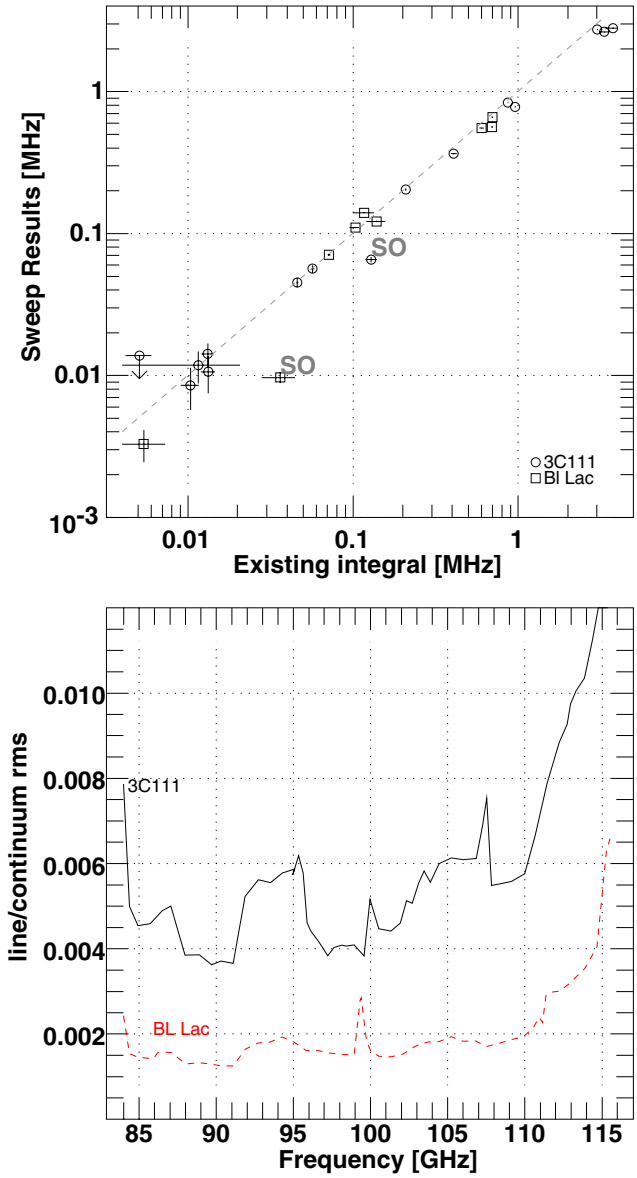

Fig. 1. Properties of the spectral sweep. *Top*: line profile integrals (equivalent widths) for the spectral sweep plotted against those previously obtained by synthesis at the Plateau de Bure Interferometer in our prior work. *Bottom*: 8-channel running mean channel-channel rms in the line/continuum ratio at 0-absorption for 3C 111 and BL Lac. The points labelled SO in the upper panel represent the 3_2–2_1 line at 99.3 GHz as discussed in Sect 2.1 of the text.

[1] See http://www.iram.fr/IRAMFR/GILDAS for more information about the GILDAS software (Pety 2005).

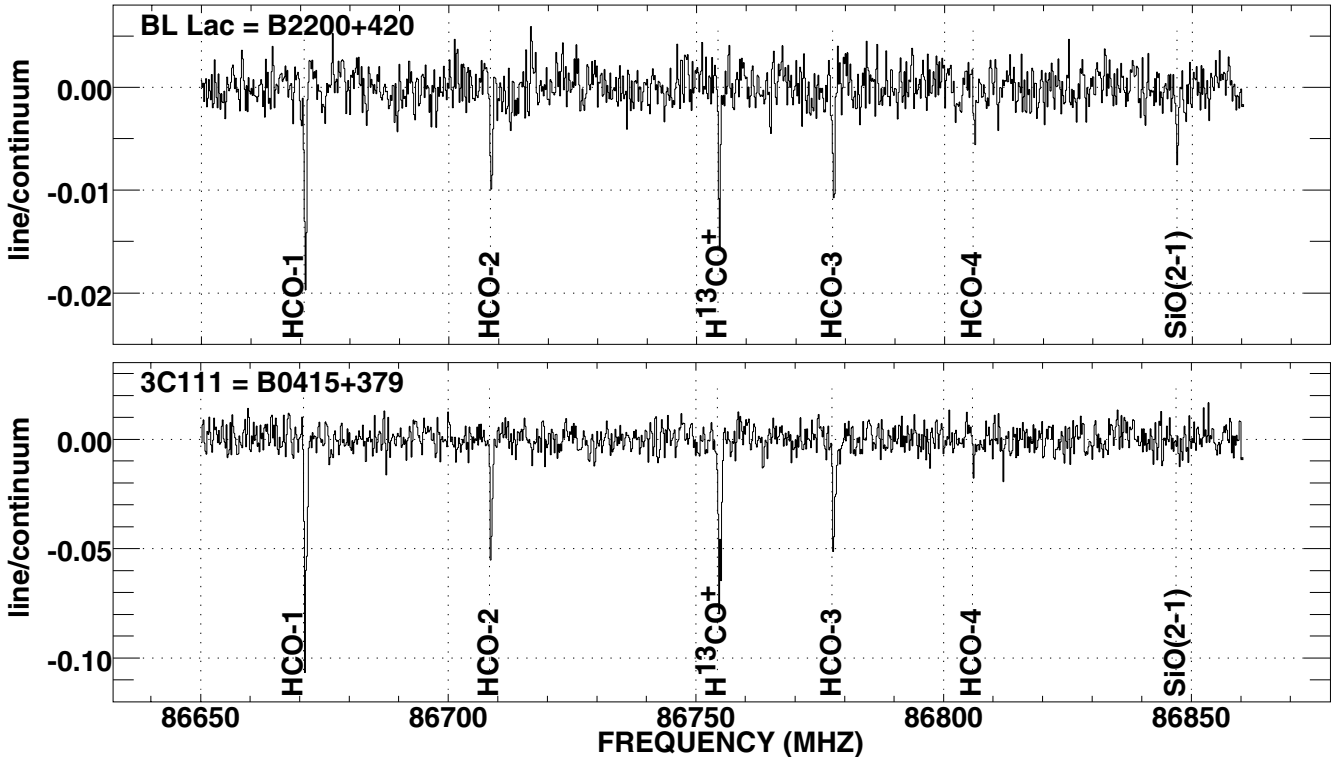

Fig. 2. Spectra of BL Lac and 3C 111 in the region of the HCO quartet. The spectral resolution is 0.195 MHz. The approximate positions of HCO, $H^{13}CO^+$ and SiO J = 2–1 transitions are marked. For spectroscopic data, see Table 2.

The SO 3–2 line at 99.3 GHz called out in Fig. 1 falls nearly on the join of two tunings where the system temperature may not have been reliably inferred by the data reduction software and was the only feature so affected.

2.2. Survey properties: rms

Figure 1 at bottom shows the rms line/continuum noise for BL Lac and 3C 111 across the frequency band surveyed. To make these plots, we calculated a running rms over 8-channel intervals in line spectra divided by the continuum and averaged this over absorption-free regions of (approximately) fixed mean rms, determined by visual inspection. When the running mean rms changed beyond twice the expected variance a new data point was created. The rms increases at the extreme of the low end because less time was spent there and more broadly at the high end because of the increased atmospheric opacity and consequent increase of system temperature. Inside the extremes there are patches in the survey with noticeably higher rms. These are caused by some combination of smaller integration time/higher system temperature and artifacts in the IF. Some of these artifacts are narrow and resemble astronomical spectral lines while others are much broader. By careful comparison of tunings and polarizations we concluded that none of the problematic features result from true astronomical signals.

Toward BL Lac $0.0015 < \sigma < 0.002$ over the region 85–110 GHz leading to a single-channel detection sensitivity $3\sigma/E_{B-V} \leq 0.02$/mag and a $3-\sigma$ detection sensitivity $\leq 0.023\ \sqrt{(\mathrm{d}V)}$/mag when integrated over a velocity interval $\mathrm{d}V$ (km s^{-1}) at 100 GHz. The same quantities obtained toward 3C 111 were $0.004 < \sigma < 0.006$ and $3\sigma/E_{B-V} \leq 0.011$/mag for the single-channel sensitivities and a $3-\sigma$ velocity-integrated sensitivity $\leq 0.014\ \sqrt{(\mathrm{d}V)}$/mag at 100 GHz.

Thus, although the intrinsic channel-channel rms noise is considerably smaller toward BL Lac owing to its higher flux during the period of observations, the signal/noise of the new detections is better toward 3C 111 owing to the higher column density. Nonetheless, the increased sensitivity toward 3C 111 did not result in the detection of any additional species beyond those also seen toward BL Lac, even tentatively. Future observations that seek to improve significantly on the current results will have to have rms $\ll 0.002$ at $E_{B-V} = 0.32$ mag and rms/$E_{B-V} \ll 0.003$ mag $^{-1}$ more generally.

2.3. Improved results for SiO and other previously-detected species

BL Lac was not included in our earlier survey of SiO J = 2–1 absorption (Lucas & Liszt 2000) so the spectrum in Fig. 2 represents the first detection of SiO in this direction; the SiO spectrum of NRAO150 is superior to that in the earlier work. SiO is one of several species (e.g. N_2H^+) whose abundances, either detections or upper limits, warrant rediscussion on the basis of the sensitivity achieved in the current work. This work is in progress.

2.4. Aperture synthesis of W49 in HCO and $H^{13}CO^+$ at the PdBI

We observed the 86.774 GHz HCO F = 1–1 line at the Plateau de Bure Interferometer for 7 h in September 2007 in the D configuration (baselines 25–100 m) and in 2008 April for 9 h in the C configuration (25–175 m) to achieve a combined spatial resolution of 4.0″ over a single primary beam pointing. The spectral resolution was 270 kHz or 0.93 km s^{-1} and the rms noise in the line/continuum ratio at 0 absorption was 0.007 with 4.2 h of

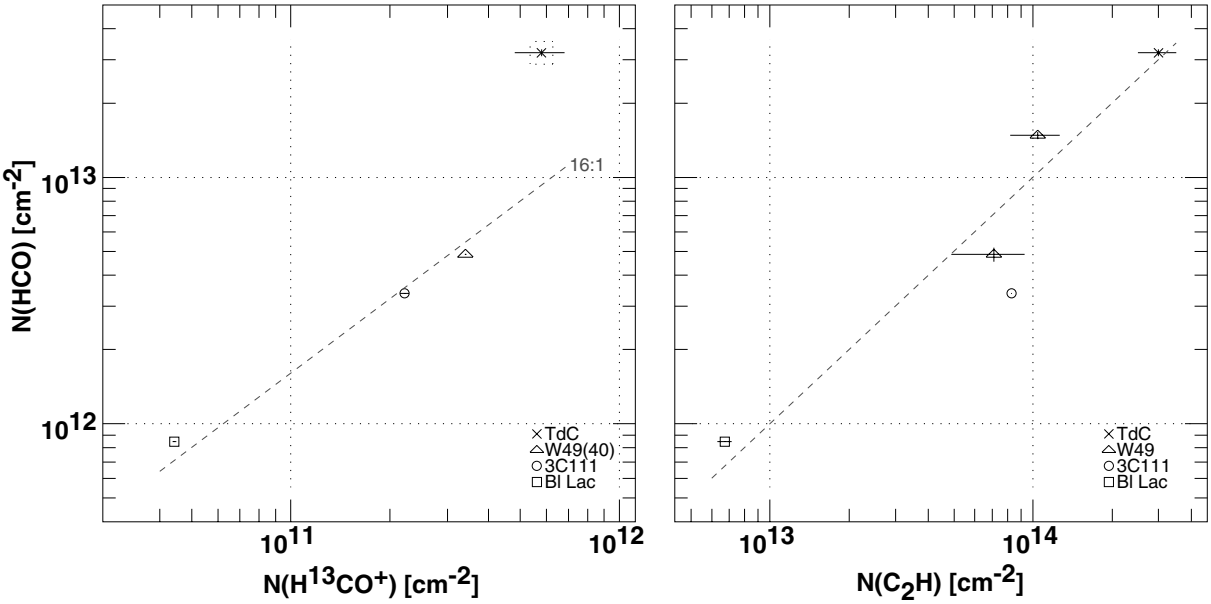

Fig. 3. Column density of HCO vs. $H^{13}CO^+$ (*left*) and C_2H (*right*). For W49 only the "spiral arm" feature at 40 km s^{-1} is shown at left using data from the present work; at right the C_2H data of Godard et al. (2010) is used for the 40 km s^{-1} and 60 km s^{-1} features. Data from the Horsehead PDR (TdC) are from Gerin et al. (2009). The dashed lines have power-law slope of unity, with proportions of 16:1 and 1:10 at *left and right*, respectively. Error bars in this and all other plots are 1σ statistical uncertainties.

Table 2. HCO 1_{01}–0_{00} transitions observed and column density-optical depth conversions[a].

Frequency	F'–F	J'–J	$A_{F',F}$	$N(X)/\int \tau dv$[b]
MHz			10^{-6} s^{-1}	cm^{-2} (km s^{-1})$^{-1}$
86 670.76	2–1	3/2–1/2	4.69	2.26×10^{13}
86 708.36	1–0	3/2–1/2	4.60	3.84×10^{13}
86 774.46[c]	1–1	1/2–1/2	4.61	3.84×10^{13}
86 805.75	0–1	1/2–1/2	4.72	1.13×10^{14}

Notes. [(a)] Spectroscopic data from `www.splatalogue.net` see Blake et al. (1984). [(b)] Assuming excitation in equilibrium with the cosmic microwave background. [(c)] This component was observed toward W49.

usable integration time. The LO was centered slightly too low in velocity for simultaneous coverage of $H^{13}CO^+$ in all of the "spiral arm" features that are seen in absorption in this direction but the strong absorption at 40 km s^{-1} was captured. All the previously known spiral arm features were seen in HCO.

3. HCO and its detection in diffuse clouds

HCO was studied extensively at H II region-molecular cloud interfaces by Snyder and Schenewerk and their collaborators (Schenewerk et al. 1988), including Ori B and W49 but its presence in diffuse and translucent clouds has not previously been noticed. Table 4 of Schenewerk et al. (1988) has $N(HCO)/N(H^{13}CO^+)$ = 1–3 generally and 10 toward NGC 2024 but they did not derive column densities for either species individually.

The spectra of HCO toward BL Lac and 3C 111 are shown in Fig. 2 and toward W49 in Fig. 4. The transitions observed and their transition probabilities are given in Table 2; the observed line depths are as expected in LTE. The HCO column densities quoted here in Table 1 were derived from a simultaneous gaussian fit to all observed transitions assuming that the excitation is in equilibrium with the cosmic microwave background. We find $N(HCO)/N(H^{13}CO^+)$ = 16 toward BL Lac, 3C 111 and the 40 km s^{-1} spiral arm cloud toward W49, much larger than the values 1–3 seen in the denser regions studied by Schenewerk et al. (1988). The abundance of HCO relative to molecular hydrogen from our work is $X(HCO) = 8 \times 10^{-10}$ if $N(H^{13}CO^+)/N(HCO^+)$ = 1/60 and $X(HCO^+) = 3 \times 10^{-9}$. This is about 10 times higher than in the dark clouds TMC-1 or B1, according to recent unpublished results (Marcelino & Bacmann, priv. comm.).

Figure 3 at right shows a comparison of N(HCO) with $N(C_2H)$ in the diffuse and spiral arm clouds at 40 and 60 km s^{-1} toward W49 using the C_2H column densities of Godard et al. (2010), and toward the Horsehead. Most of these have abundance ratios $N(HCO)/N(C_2H) \approx 0.1$ with a three times smaller value toward 3C 111, which has a higher than normal ratio $N(C_2H)/N(HCO^+)$. For the Horsehead the peaks of the spatial distributions of C_2H and HCO coincide just inside the illuminated edge of the PDR while the peak of HCO^+ lies further inside the neutral region. The Horsehead has a much higher ratio of $N(HCO)/N(H^{13}CO^+)$ in Fig. 3 at left because the edge-on viewing geometry allows us to distinguish the HCO and HCO^+ peaks. If the Horsehead were observed face-on its $HCO/H^{13}CO^+$ ratio would most likely resemble much more closely that seen in the diffuse and spiral arm clouds because all of the material would be observed along the same sighlines. Whether such a segregation occurs in the diffuse and spiral arm clouds is impossible to discern.

Coincidence of the HCO and hydrocarbon peaks in the Horsehead may be ascribed to the formation mechanism for HCO, $O + CH_2 \rightarrow HCO + H$: Gerin et al. (2009) found that a rapid rate for this reaction was required to explain the observed abundances. In turn, CH_2 formation is initiated by the endothermic reaction $C^+ + H_2$ but C^+ does not survive into dense molecular gas after carbon is converted to CO. Therefore HCO is most

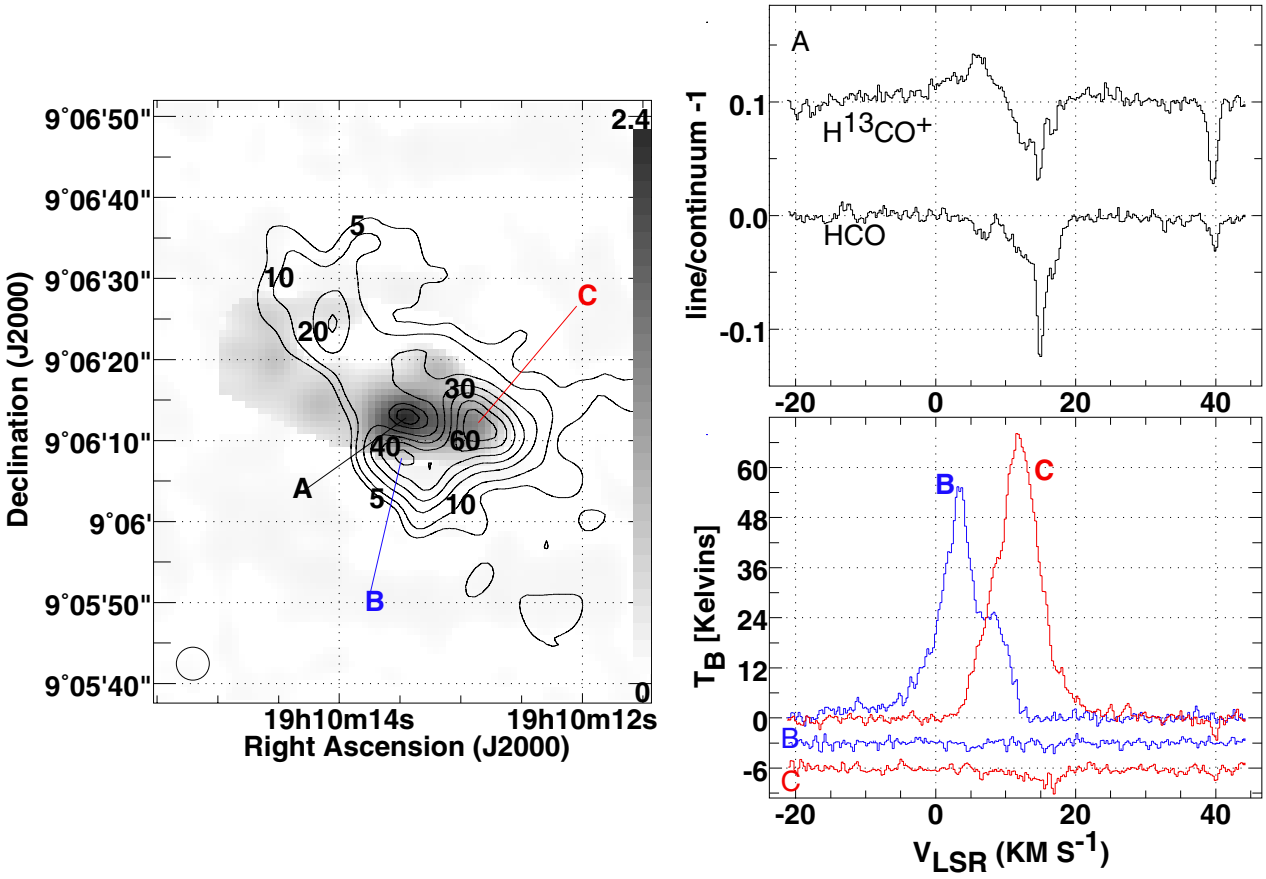

Fig. 4. W49 continuum, HCO $F = 1–1$ and $H^{13}CO^+$ emission and absorption spectra. *Left*: 86.8 GHz continuum (grayscale; peak =2.5 Jy) and $H^{13}CO^+$ emission (contours of integrated brightness temperature in units of Kelvins km s^{-1}). The 4″ synthesized HPBW is shown inset at *lower left*. *Right top*: spectra of $H^{13}CO^+$ and HCO toward the continuum peak labelled position "A" at left. *Right bottom*: emission spectra at off-continuum positions "B" (blue in electronic media) and "C" (red). Spectra showing strong emission are $H^{13}CO^+$, those without are spectra of HCO.

properly viewed as existing in interface regions where the density is comparatively high and a substantial H_2 fraction is present but carbon remains largely in the form of C^+.

Figure 4 illustrates how HCO is present in the gas within the W49 HII region-molecular cloud complex as a whole but does not persist into the denser neutral regions. The maps at left superpose contours of integrated $H^{13}CO^+$ emission upon the continuum in greyscale, noting three positions A (the continuum), B and C at which line profiles are shown at right. $H^{13}CO^+$ at positions B and C (lower right) shows blue and red-shifted emission features, respectively (with slight overlap), corresponding to the blue-shifted $H^{13}CO^+$ emission and red-shifted absorption seen toward the continuum at position A. Thus the overall morphology can be explained by a disk geometry whose blue-shifted southeastern part is situated behind the continuum, so representing infalling material. By contrast, HCO at position A toward the continuum shows strong red-shifted absorption but no blue-shifted emission from the denser gas behind the continuum. Likewise, HCO shows no detectable emission off the continuum at positions B or C. HCO exists only in lower density portions of the molecular gas where the abundance of C^+ is relatively large but the molecular excitation of HCO is relatively weak.

4. c-C_3H and its detection in diffuse clouds

The discovery spectra of c-C_3H in diffuse and translucent clouds are shown in Fig. 5. The transitions observed and their transition probabilities are given in Table 3; the observed line depths are as expected in LTE. The column densities quoted here in Table 1 were derived from a simultaneous gaussian fit to all observed transitions assuming that all excitation is in equilibrium with the cosmic microwave background.

Table 3. c-C_3H $2_{12}–1_{11}$ transitions observed and column density-optical depth conversions[a] .

Frequency	$F'–F$	$J'–J$	$A_{F',F}$	$N(X)/\int \tau dv^b$
MHz			10^{-5} s^{-1}	cm^{-2} (km s^{-1})$^{-1}$
91494.35	3–2	5/2–3/2	1.545	1.02×10^{13}
91497.61	2–1	5/2–3/2	1.545	1.42×10^{13}
91692.75	1–0	3/2–1/2	1.545	2.39×10^{13}
91699.47	2–1	3/2–1/2	1.545	1.43×10^{13}

Notes. [(a)] Spectroscopic data from Chandra et al. (2007). [(b)] Assuming excitation in equilibrium with the cosmic microwave background.

Figure 6 compares the observed column densities of c-C_3H with those of $H^{13}CO^+$, ortho-c-C_3H_2 and C_2H. The values quoted for the Horsehead in Fig. 6 are from the singledish IRAM 30 m observations of Pety et al. (2012) at lower spatial resolution than those shown in Fig. 4. The quasar absorption sightlines and TMC-1 have similar N(c-C_3H)/N($H^{13}CO^+$) ≈ 3, N(c-C_3H)/N(o-c-C_3H_2) ≈ 0.1 and N(c-C_3H)/N($H^{13}CO^+$) ≈ 0.01.

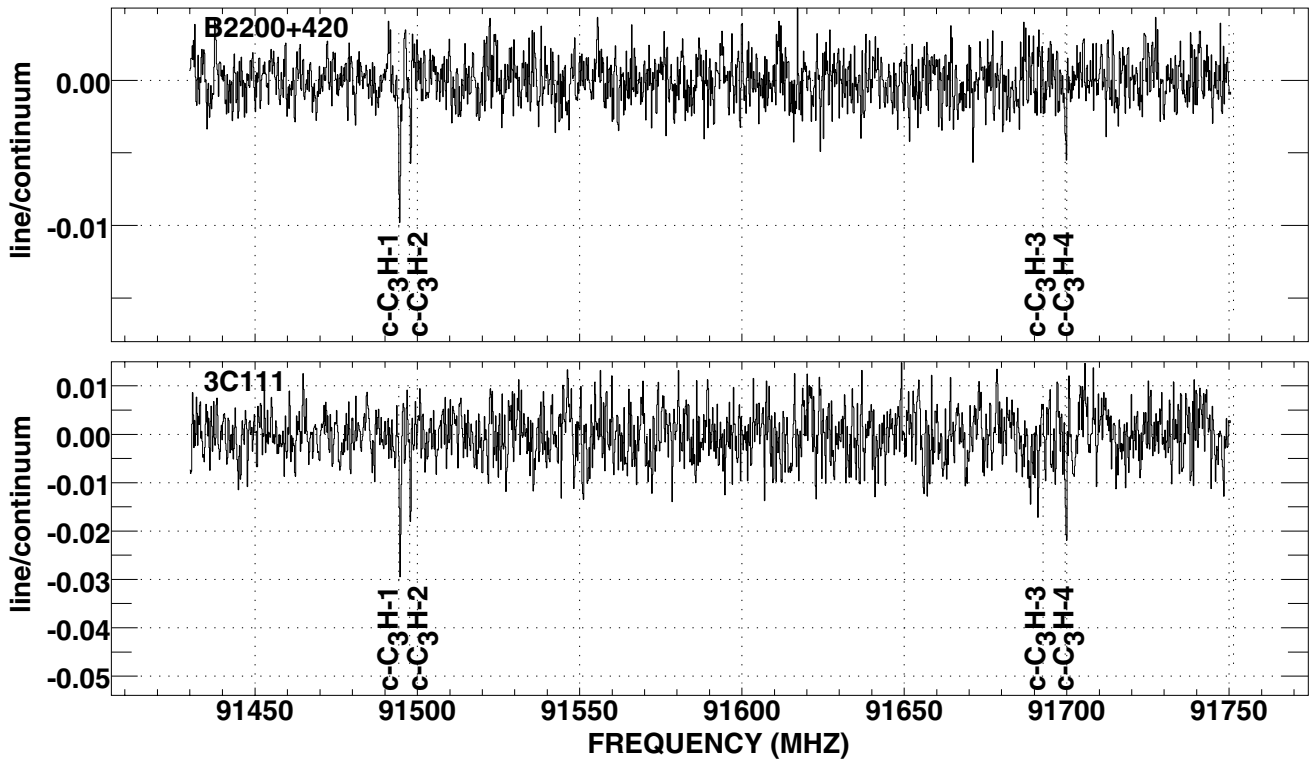

Fig. 5. Spectra of BL Lac and 3C 111 in the region of the c-C_3H quartet. The spectral resolution is 0.195 MHz. For spectroscopic data, see Table 3.

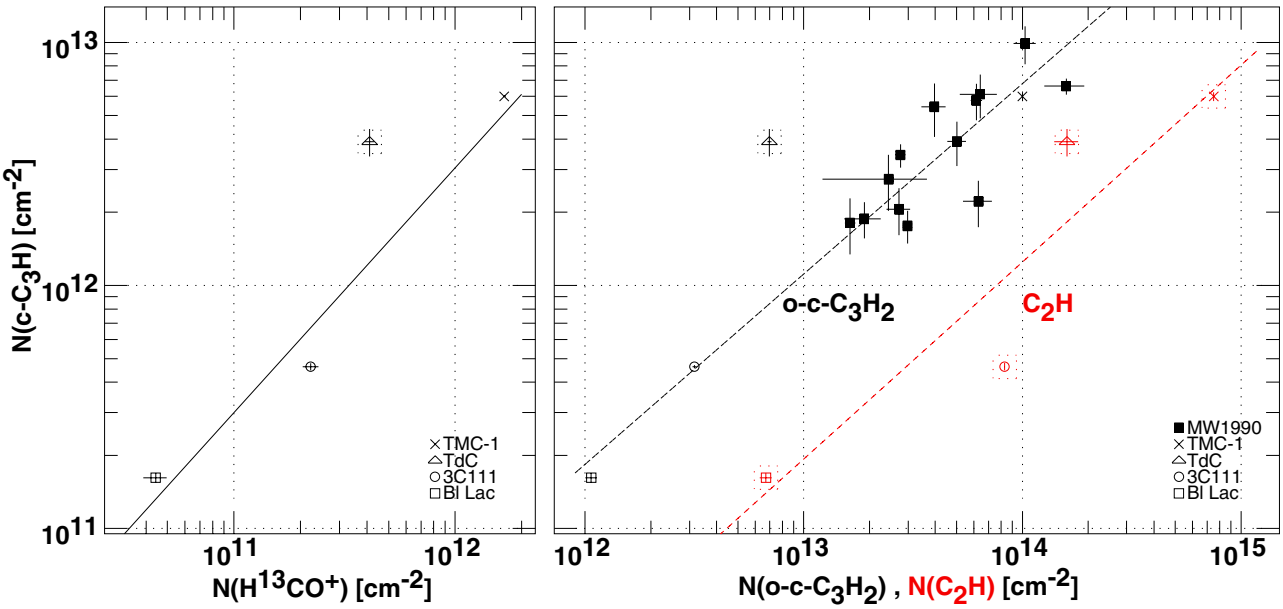

Fig. 6. Column density of c-C_3H vs. $H^{13}CO^+$ (at *left*), and C_3H_2 and C_2H (*right*). Data for the hydrocarbons toward the Horsehead nebula (TdC) are from Pety et al. (2012). Data for TMC-1 are from Ohishi et al. (1992). The c-C_3H survey data of Mangum & Wootten (1990) are shown at *right*, labelled "MW1990". The solid line at *left* has power-law slope 1; at *right*, both lines have slope 0.8.

N(c-C_3H) for the Horsehead is high by a factor two-four with regard to $H^{13}CO^+$ and *c*-C_3H_2, and perhaps somewhat high with respect to C_2H as well.

Mangum & Wootten (1990) noted that the relative abundances of c-C_3H and c-C_3H_2 varied little with environment, whether in dark or giant molecular clouds, HII region-molecular cloud complexes, etc. Our data greatly extend this conclusion downward in column density and across chemical families. At left in Fig. 6 it is seen that N(c-C_3H)/N($H^{13}CO^+$) = 3 toward TMC-1 and the two blazars observed here, over a range of a factor 40 in column density. At right the regression lines have power-law slope 0.80, so that N(c-C_3H)/N(C_3H_2) and N(c-C_3H)/N(C_2H) vary by a factor ±2 about a common mean over a factor 100 in N(c-C_3H_2) and N(C_2H).

From the lack of variability in their abundance ratio, Mangum & Wootten (1990) inferred that c-C_3H and C_3H_2 shared a common chemical antecedent $C_3H_3^+$. Although this may be true, Fig. 6 suggests that c-C_3H is simply another species, like HCO^+, C_2H, and C_3H_2, whose abundance relative to H_2 varies little in the ISM at large.

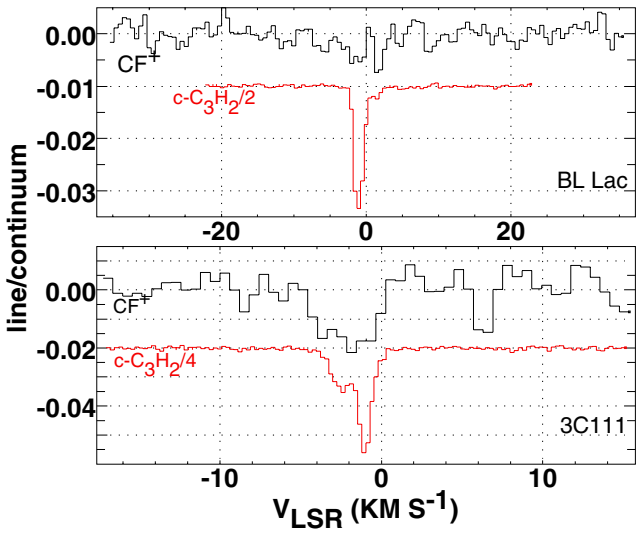

Fig. 7. CF^+ spectra toward BL Lac (*upper*) and 3C 111 (*lower*). The velocity axis corresponds to the mean LTE intensity-weighted centroid of the two hyperfine components noted in Table 4. Shown for comparison are scaled spectra of the 18.3 GHz transition of c-C_3H_2 from Liszt et al. (2012). For spectroscopic data, see Table 4.

Table 4. CF^+ transitions observed and column density-optical depth conversions[a] .

Frequency MHz	F'–F	J'–J	$A_{F',F}$ 10^{-6} s^{-1}	$N(\mathrm{X})/\int \tau dv^b$ cm^{-2} (km s^{-1})$^{-1}$
102587.189	1/2–1/2	1–0	4.82	4.04×10^{13}
102587.533	3/2–1/2	1–0	4.82	2.02×10^{13}

Notes. [(a)] Spectroscopic data from Guzmán et al. (2012b) and www.splatalogue.net; [(b)] assuming excitation in equilibrium with the cosmic microwave background.

5. CF^+ and its detection in diffuse clouds

CF^+ has previously been observed only in regions of much higher density, the Orion Bar (Neufeld et al. 2006) and the Horsehead (Guzmán et al. 2012a,b). The discovery spectra of CF^+ in diffuse clouds are shown in Fig. 7 and the transitions observed and their transition probabilities are given in Table 4. The low spectral resolution of the sweep data, combined with the 0.34 MHz or 1.01 km s^{-1} separation of the two hyperfine components prevents a reliable determination of the relative strengths of the kinematic components toward 3C 111. The column densities quoted here in Table 1 were derived by integrating over the observed profiles.

Figure 8 shows that $N(CF^+)$ increases with $N(H^{13}CO^+)$ and $N(C_2H)$, although more slowly than linearly (power law slopes 0.6 and 0.4 respectively). Figure 8 also shows the prediction of Neufeld & Wolfire (2009) that $N(CF^+) \approx 4.5 \times 10^{11}$ cm^{-2} for $A_V \gtrsim 1$ with most fluorine in HF in the H_2-bearing regions. The conversion of carbon to CO and the abrupt depletion of gas phase fluorine at $A_V > 1$ mag both act to confine CF^+ at $A_V < 1$ mag and to limit $N(CF^+)$ in the models of Neufeld & Wolfire (2009).

CF^+ forms from HF *via* $C^+ + HF \rightarrow CF^+ + H$ with a rate constant $k_1 = 7.2 \times 10^{-9}(T/300)^{-0.15}$ cm^3 s^{-1} and is destroyed by recombination with electrons with a recombination coefficient $\alpha_1 = 5.3 \times 10^{-8}(T/300)^{-0.8}$ cm^3 s^{-1}. If C^+ is the dominant source of free electrons it follows that $n(CF^+)/n(HF) = 0.136\ (T/300)^{0.65}$ with most gas-phase fluorine in HF.

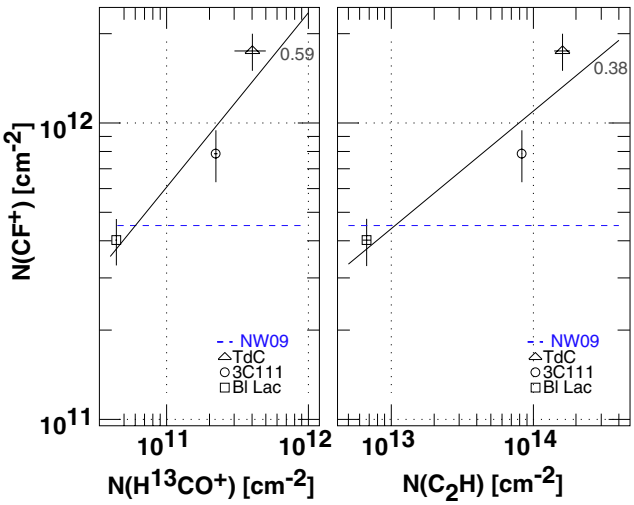

Fig. 8. Column density of CF^+ vs. $H^{13}CO^+$ (at *left*) and C_2H (*right*). Data for the Horsehead nebula (TdC) are from Guzmán et al. (2012a). The prediction $N(CF^+) \approx 4.5 \times 10^{11}$ cm^{-2} at $A_V \gtrsim 1$ mag of Neufeld & Wolfire (2009) is shown as a blue dashed horizontal line. The power law slopes of the best-fit lines (0.59, 0.38) are noted.

We know that C^+ survives as the dominant form of carbon at and well beyond $A_V = 1$ mag because of the strong fractionation of ^{13}C into ^{13}CO that is seen toward BL Lac and 3C 111 (Liszt & Lucas 1998); substantial amounts of gas-phase fluorine in the form of HF must also survive beyond $A_V = 1$ mag to provide the behaviour seen in Fig. 8. If the fractional abundances of HCO^+ and C_2H with respect to H_2 are about constant and the kinetic temperature does not vary substantially, the depletion of gas phase fluorine (HF) would vary approximately as $A_V{}^{-1/2}$. If the temperature were assumed to decline at higher A_V, the depletion of fluorine would have to be even weaker in order to compensate for the smaller equilibrium CF^+/HF ratio, which varies as $T^{0.65}$ according to the simple chemical scheme detailed above (Neufeld & Wolfire 2009).

6. Summary

We surveyed the 84–116 GHz 3 mm spectrum in absorption against the compact extragalactic mm-continuum sources BL Lac and 3C 111 as noted in Table 1 at 195 kHz spectral resolution (0.6 km s^{-1} at 100 GHz), achieving an rms noise level $\delta_\tau \approx 0.002$ at $E_{B-V} = 0.32$ mag ($A_V = 1$ mag) toward BL Lac and $\delta_\tau / E_{B-V} \approx 0.003$ mag^{-1} overall. HCO, c-C_3H and CF^+ were detected in absorption toward both sources and HCO was also found in the diffuse "spiral-arm" clouds in the galactic plane in front of W49. We discussed observational aspects of their chemistry in Sects. 3–5.

c-C_3H is notable for having a nearly fixed abundance with respect to HCO^+, C_2H and c-C_3H_2 over a wide range of column density, even across the divide between the diffuse and dark or giant molecular clouds. The increase in $N(CF^+)$ beyond $A_V = 1$ mag shows that both fluorine and C^+ are abundant in the gas phase at such extinctions but conclusions about the depletion of fluorine are sensitive to assumptions about the temperature profile. The relative abundance ratio $N(HCO)/N(H_2)$ is higher in diffuse than dark or dense molecular gas, consistent with its prior interpretation as a species requiring both C^+ and H_2 for its formation via the reaction $O + CH_2 \rightarrow HCO + H$.

No other new species are present in the spectra toward BL Lac (A_V= 1 mag) at a 5-sigma optical depth limit of 0.01

in any single feature, suggesting that the hunt for new species in diffuse clouds in the radio domain will be most profitably conducted in the cm-wave region below 30 GHz where the more heavily-populated lower-lying energy levels of heavier polyatomic molecules are most readily accessible.

Appendix A: Upper limits on undetected species

In most cases we have examined, the upper limits we can derive for undetected species are not sufficiently sensitive to be interesting. For instance, we derive 3σ upper limits $N(\text{l-}C_3H^+) < 2.3 \times 10^{11}$ cm^{-2} and $N(\text{l-}C_3H^+) < 6.0 \times 10^{11}$ cm^{-2} toward BL Lac and 3C 111, respectively, but these are at most barely below the value $N(\text{l-}C_3H^+) = 4.8 \times 10^{11}$ cm^{-2} for the Horsehead (Pety et al. 2012) whose column densities are generally 3–10 times larger. For the neutral l-C_3H the upper limits that may be derived from this work are not competitive with those accessible at lower frequency using the VLA and likewise with C_4H (Liszt et al. 2012).

One species that is better-constrained is H_2CS whose J = 3–2 transitions appear at 101.5 and 104.6 GHz. We find 3σ limits $N(H_2CO)/N(H_2CS) > 11 \pm 2.5$ and $N(H_2CO)/N(H_2CS) > 32 \pm 8$ toward BL Lac and 3C 111 respectively using the prior results of Liszt et al. (2006), compared to $N(H_2CO)/N(H_2CS) = 7$ toward TMC-1 (Ohishi et al. 1992).

Acknowledgements. The National Radio Astronomy Observatory is a facility of the National Science Foundation operated under cooperative agreement by Associated Universities, Inc. IRAM is operated by CNRS (France), the MPG (Germany) and the IGN (Spain). This work was partly funded by grant ANR-09-BLAN-0231-01 from the French *Agence Nationale de la Recherche* as part of the SCHISM project. We thank the editor, Malcolm Walmsley, and the anonymous referee for their comments.

References

Blake, G. A., Sastry, K. V. L. N., & de Lucia, F. C. 1984, J. Phys. Chem., 80, 95
Chandra, S., Shinde, S. V., Kegel, W. H., & Sedlmayr, E. 2007, A&A, 467, 371
Falgarone, E., Godard, B., Cernicharo, J., et al. 2010, A&A, 521, L15
Gerin, M., Goicoechea, J. R., Pety, J., & Hily-Blant, P. 2009, A&A, 494, 977
Gerin, M., de Luca, M., Goicoechea, J. R., et al. 2010, A&A, 521, L16
Gerin, M., Levrier, F., Falgarone, E., et al. 2012, Roy. Soc. London Philos. Trans. Ser. A, 370, 5174
Godard, B., Falgarone, E., Gerin, M., Hily-Blant, P., & de Luca, M. 2010, A&A, 520, A20
Godard, B., Falgarone, E., Gerin, M., et al. 2012, A&A, 540, A87
Gratier, P., Pety, J., Guzmán, V., et al. 2013, A&A, 557, A101
Guzmán, V., Pety, J., Gratier, P., et al. 2012a, A&A, 543, L1
Guzmán, V., Roueff, E., Gauss, J., et al. 2012b, A&A, 548, A94
Liszt, H. S., & Lucas, R. 1998, A&A, 339, 561
Liszt, H., Lucas, R., & Pety, J. 2006, A&A, 448, 253
Liszt, H., Sonnentrucker, P., Cordiner, M., & Gerin, M. 2012, ApJ, 753, L28
Lucas, R., & Liszt, H. S. 2000, A&A, 355, 327
Mangum, J. G., & Wootten, A. 1990, A&A, 239, 319
Neufeld, D. A., & Wolfire, M. G. 2009, ApJ, 706, 1594
Neufeld, D. A., Schilke, P., Menten, K. M., et al. 2006, Astrophys., 454, L37
Neufeld, D. A., Falgarone, E., Gerin, M., et al. 2012, A&A, 542, L6
Ohishi, M., Irvine, W., & Kaifu, N. 1992, in Astrochemistry of cosmic phenomena: Proc. of the 150th Symp. IAU, held at Campos do Jordao, Sao Paulo, Brazil, August 5–9, 1991, ed. P. D. Singh (Dordrecht: Kluwer), 171
Pety, J. 2005, in SF2A-2005: Semaine de l'Astrophysique Francaise, Conf. Ser., eds. F. Casoli, T. Contini, J. M. Hameury, & L. Pagani (EDP Sciences), 721
Pety, J., Gratier, P., Guzmán, V., et al. 2012, A&A, 548, A68
Schenewerk, M. S., Jewell, P. R., Snyder, L. E., Hollis, J. M., & Ziurys, L. M. 1988, ApJ, 328, 785
Schlegel, D. J., Finkbeiner, D. P., & Davis, M. 1998, ApJ, 500, 525